JOURNAL OF MATERIALS SCIENCE 29 (1994) 835–843

Effects of grain size and specimen geometry on the transformation and *R*-curve behaviour of 9Ce-TZP ceramics

T. LIU, Y.-W. MAI, M. V. SWAIN
Centre for Advanced Materials Technology, Department of Mechanical Engineering, University of Sydney, New South Wales 2006, Australia

G. GRATHWOHL
Institut für Keramik im Maschinenbau, University Karlsruhe, Haid-und-Neu Strasse 7, W-7500 Karlsruhe 1, Germany

Transformation and *R*-curve behaviour have been investigated in 9 mol% Ce-TZP ceramics with different grain sizes. Both single-edge notched beam and short double-cantilever beam specimens were tested to measure the crack-resistance curves. The size and shape of the transformation zone not only depend on grain size, but are also strongly influenced by the specimen geometry. This different transformation behaviour has led to different crack-resistance curves. These experimental results are discussed in terms of the thermodynamics of transformation, the effect of autocatalytic transformation, and fracture mechanics.

1. Introduction

One of the most important features of transformation-toughened zirconia-based ceramics is the increasing crack-resistance (*R*-curve) behaviour caused by the crack-shielding effect due to the stress-induced t–m transformation around the crack tip. This toughening behaviour has been successfully investigated both theoretically [1, 2] and experimentally [3–6] for the Mg-PSZ, Y-TZP and ZTA ceramics. Some recent studies [7–9] have demonstrated that Ce-TZP ceramics exhibit pronounced transformation plasticity leading to high fracture toughness in the range 12–18 MPa $m^{1/2}$. However, the shapes of the transformation zones surrounding cracks in the Ce-TZPs are very different from those in other zirconia-based ceramics. In Mg-PSZ ceramics the zone extends approximately equal distances ahead and to the side of the crack, whereas in Ce-TZPs the zone is very elongated. The grain-size dependence of the transformation behaviour in Ce-TZPs has also been investigated showing a marked increase of the t–m transformation zone size with increasing grain size [9].

In the present work, the transformation and the crack-resistance (*R*-curve) behaviour of a 9 mol% Ce-TZP ceramic and the influence of grain size and specimen geometry were investigated. Very different transformation zone size, zone shape and, consequently, different *R*-curve behaviour have been found for different grain size and specimen geometries.

2. Experimental work procedure

The materials for testing were prepared from a single batch of CeO_2–ZrO_2 powder (Ce-14, United Ceramics Ltd., Stafford, UK) containing 9 mol% CeO_2. The powder was first uniaxally pressed at 6 MPa in a hard metal die to produce rectangular plates which were isostatically pressed at 200 MPa. The plates were then sintered at temperatures between 1400 and 1550 °C with heating and cooling rates of 3 °C min^{-1}.

Single-edge notched bend (SENB) and short-double-cantilever-beam (s-DCB) specimens were cut and ground from the sintered plates. The sizes of the SENB and the short-DCB specimens were $5 \times 10 \times 45$ ($t \times w \times L$) and $6.5 \times 32 \times 40$ ($t \times h \times w$) mm^3, respectively, which are shown schematically in Fig. 1a. One side of both the SENB and short-DCB specimens was polished. For the three-point bend test on the SENB specimens, a natural sharp crack was generated by the so-called "bridge method" [10]. In the short-DCB test the samples were precracked by initiating a sharp crack from a Chevron-like prenotch. These specimens were then annealed in air at 800–1200 °C to annihilate

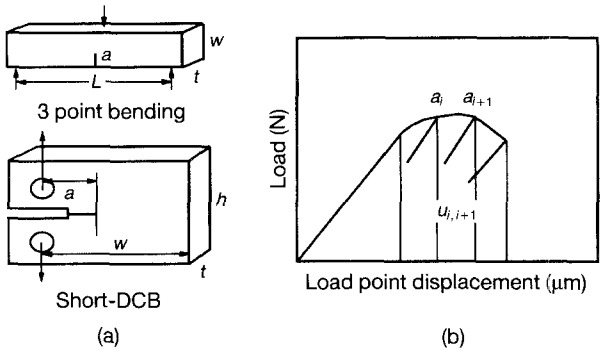

Figure 1 (a) Schematic drawings of the SENB and s-DCB specimens; and (b) typical load–load point displacement curves.

0022–2461

the t–m transformation which had taken place during precracking. In both specimen types the initial crack length to sample width ratio, a_0/w, was chosen at about 0.3 and the crosshead rate of the Instron testing machine was kept at about 1 $\mu m\,s^{-1}$. The load–point displacement was measured by a clip gauge and a LVDT in the s-DCB and SENB geometries, respectively. Crack growth was measured from the polished surface optically with a travelling microscope with an accuracy of $\pm$ 0.01 mm. The crack–resistance curve was calculated using both stress intensity factor, K, and fracture energy, J-integral, approaches.

For the SENB geometry, K_I is given by

$$K_I = \frac{3PL}{2tw^2} a^{1/2} Y\left(\frac{a}{w}\right) \quad (1)$$

where P is applied load, L (40 mm) span width, t thickness, w specimen width, a crack length, and $Y(a/w)$ is a function of a/w and can be obtained from stress intensity factor handbooks [11, 12].

The J-integral is calculated using the following equation [13]

$$J_{i+1} = J_i \frac{w - a_{i+1}}{w - a_i} + \frac{2U_{i,i+1}}{t(w - a_i)} \quad (2)$$

where $U_{i,i+1}$ for the crack interval $(a_{i+1} - a_i)$ is shown in Fig. 1b.

For the short-DCB geometry, K_I is given by [14]

$$K_I = \frac{P}{tw^{1/2}} \left[\frac{(2 + a/w)}{1 - (a/w)^{3/2}}\right] f(a/w) \quad (3)$$

and $f(a/w)$ is taken from Srawley and Gross [15]. The J-integral is obtained from [15, 16]

$$J_{i+1} = \left(J_i + \frac{\eta_i}{w - a_i} \frac{U_{i,i+1}}{t}\right) \times \left[1 - \frac{\gamma_i}{w - a_i}(a_{i+1} - a_i)\right] \quad (4)$$

where $U_{i,i+1}$ is shown in Fig. 1b, η_i and γ_i are given by [17]

$$\eta_i = 1.6 + 2.65(1 - a_i/w)^2 \quad (5)$$

$$\gamma_i = -0.2 + 4.3(1 - a_i/w) \quad (6)$$

Using the K_I values calculated from Equations 1 and 3 for the SENB and s-DCB geometries, the elastic parts of the J-integral, J_{el}, were also calculated by

$$J_{el} = K_I^2 \frac{(1 - \nu^2)}{E} \quad (7)$$

where ν is Poisson's ratio and E is Young's modulus. At equilibrium crack growth $K_I = K_R$ and $J = J_R$ (see Mai and Lawn [18]).

3. Results

3.1. Transformation behaviour

Table I shows the sintering conditions, the grain sizes obtained and the relative density of the Ce-TZP materials. With increasing sintering temperature the grain sizes were increased. Fig. 2 shows the load–load point displacement curves for the Ce-TZP-I and Ce-TZP-II materials in the SENB and short-DCB geometries. While the samples with a grain size of 1.1 μm

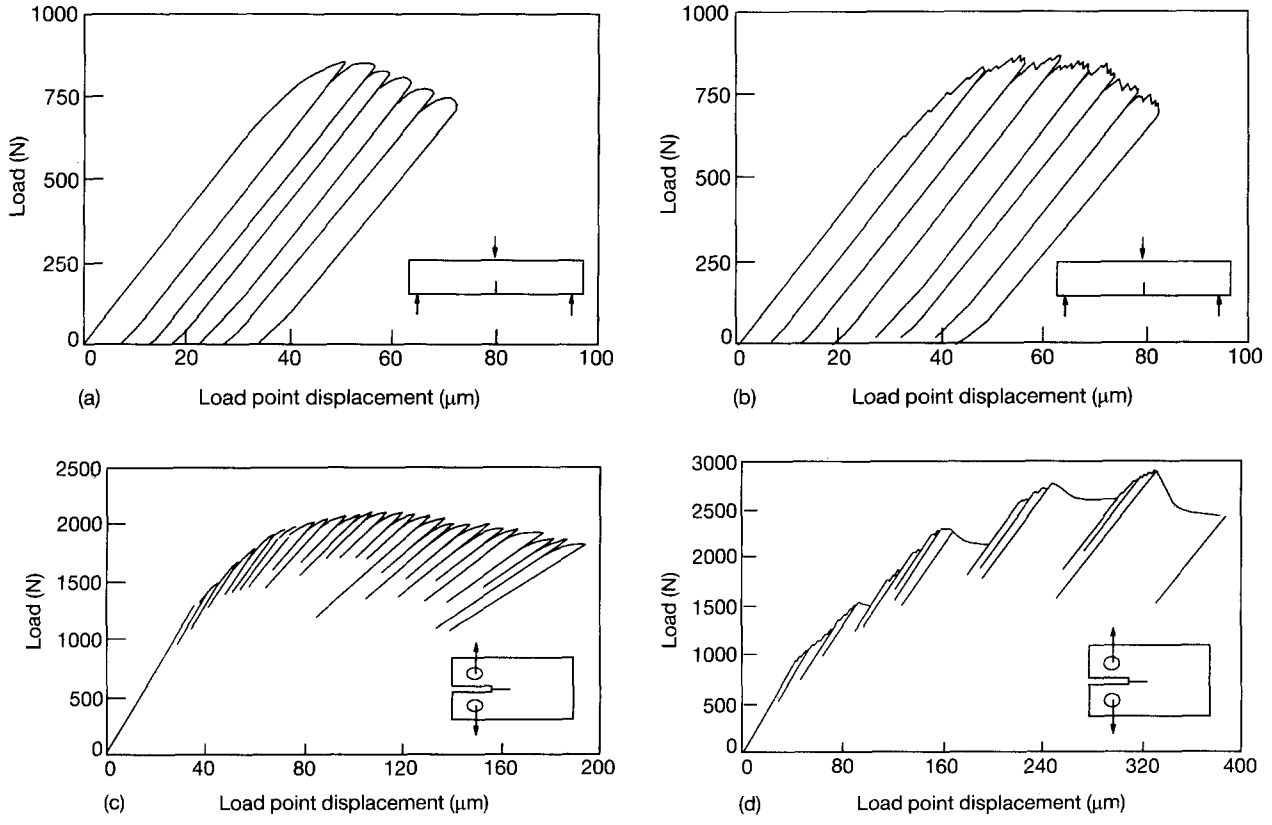

Figure 2 Load–load point displacement curves of (a) Ce-TZP-I in three-point bending, (b) Ce-TZP-II in three-point bending, (c) Ce-TZP-I in short-DCB test, (d) Ce-TZP-II in short-DCB test.

TABLE I Sintering conditions, grain size and relative densities of the Ce-TZP materials

Materials	Sintering conditions		Average grain size (μm)	Rel. density (% TD)
	(°C)	(h)		
Cc-TZP-I	1400	1	1.14	94
Ce-TZP-II	1450	1	1.62	97
Ce-TZP-III	1500	1	2.22	98
Ce-TZP-IV	1550	1	3.00	97

show continuously increasing inelastic deformations (Fig. 2a and c), the samples with a grain size of 1.6 μm (and those of larger grain sizes) undergo stepwise plastic deformation and localized intensity as shown in Fig. 2b and d. Similar behaviour was also observed by Grathwohl and Liu [9] which was believed to be caused by the autocatalytic effect of the stress-induced t–m transformation and its grain-size dependence. Figs 3 and 4 show the t–m transformation zones of both the SENB and short-DCB geometries, respectively, with different grain sizes. (Note that these transformation zones correspond to the plateau values of the K_R–Δa and the J_R–Δa curves in Figs 9 and 11). While the Ce-TZP-I material exhibits a very small transformation zone size, the other three materials show a dramatic increase in their transformation zone size in both SENB and short-DCB geometries. These results show that the transformation behaviour is dependent both on grain size and specimen geometry as shown in Fig. 5. The abrupt increase of the transformation zone size with increasing grain size has already been reported previously [9]. The new phenomenon given in this work, however, is the marked difference of the transformation zones of the SENB and s-DCB geometries both in size and in shape. Figs 6 and 7 show the development of the transformation zones with crack extensions in both the SENB and short-DCB geometries, respectively, for the Ce-TZP-II and Ce-TZP-III materials. The elongated zone shape in the SENB geometry and the large zone volume with long and slender transformation "tails" in the s-DCB geometry are clearly visible. Crack deflection and crack branching as a result of microcracking in the t–m transformation zone were also observed with optical microscopy in the Ce-TZP-IV material with a grain size of 3.0 μm (Fig. 8). However, with the other Ce-TZP materials with smaller grain size, such crack branching and crack deflection due to microcracking in the transformation zone cannot be observed either optically or in the SEM.

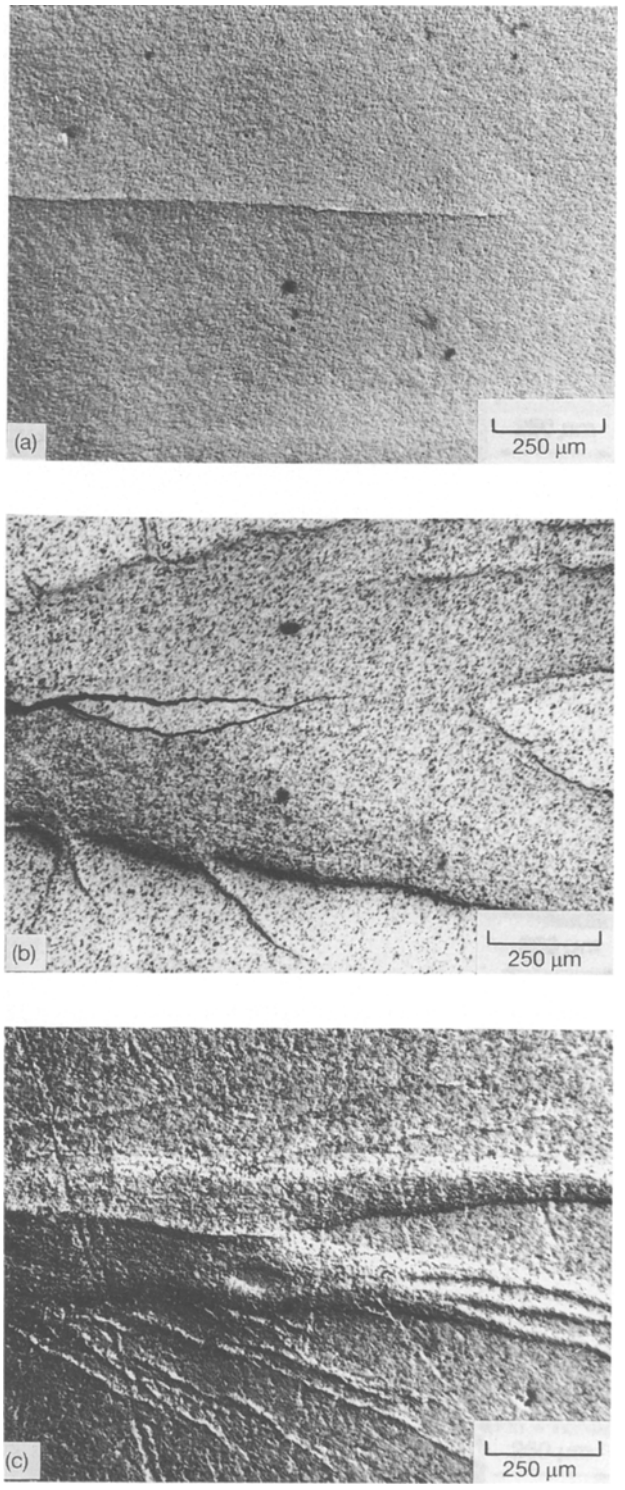

Figure 3 Transformation zones in SENB specimens of (a) Ce-TZP-I; (b) Ce-TZP-II; (c) Ce-TZP-III.

3.2. Crack-resistance curves

Fig. 9 shows the crack-resistance, K_R, curves for Ce-TZP-I measured in the SENB and s-DCB geometries. Because the transformation zone size is very small compared to the specimen size, the K-concept can be used for the characterization of the crack-resistance behaviour. It is seen that K_R increases from about 10 MPa $m^{1/2}$ to 18 MPa $m^{1/2}$ over a crack growth of about 5 mm. There is good agreement between the K_R curves measured with these two specimen geometries. Additional data obtained from compact tension specimens (CT) also support these results. Fig. 10 shows the crack-resistance curve of a Ce-TZP-I (s-DCB) specimen after it was reannealed following a previous R-curve experiment. The initial value of the R-curve after reannealing is virtually identical to that of the previous R-curve. This indicates that the increasing R-curve in this material is mainly caused by crack-shielding due to the t–m transformation during crack extension.

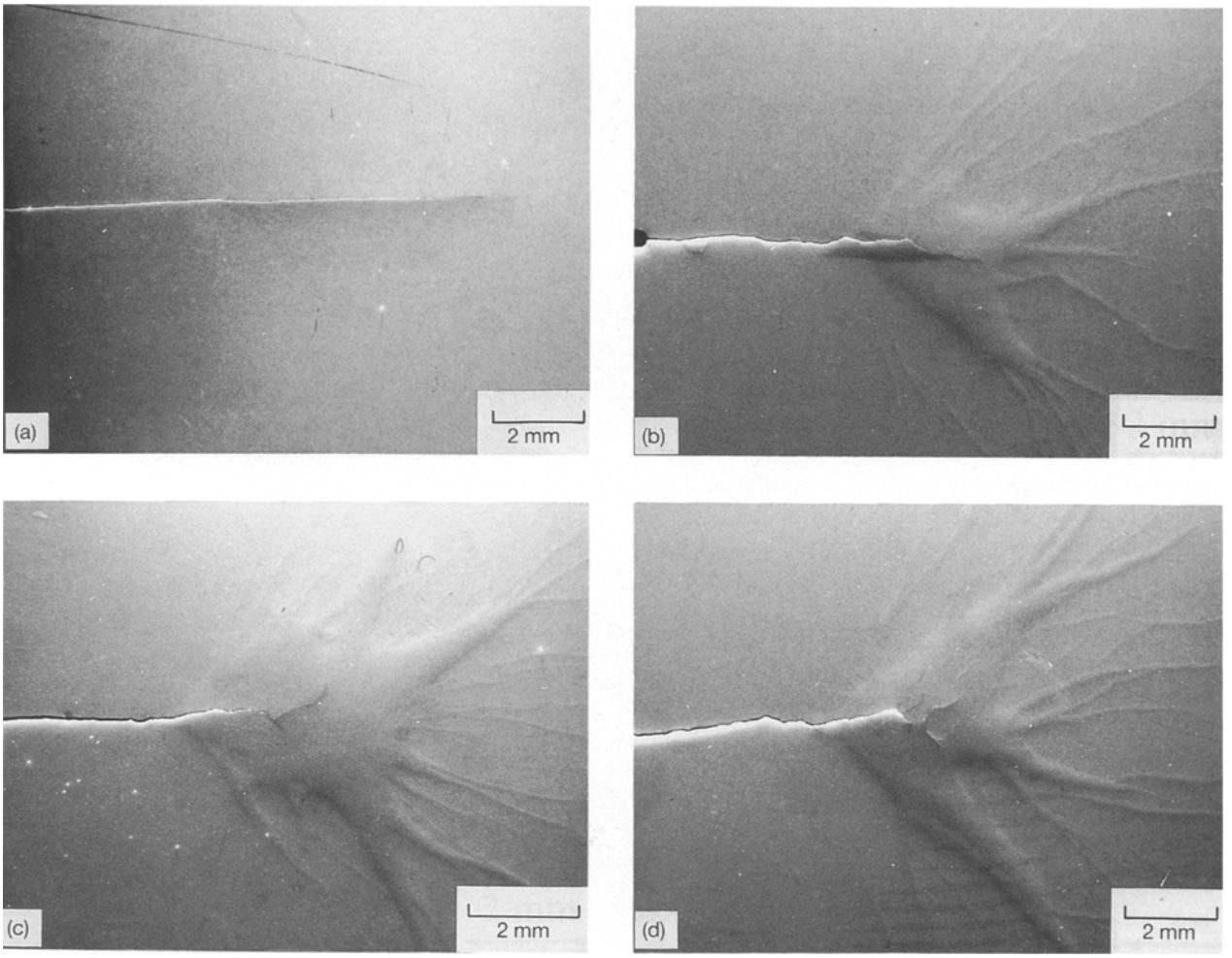

Figure 4 Transformation zones in s-DCB specimens of (a) Ce-TZP-I; (b) Ce-TZP-II; (c) Ce-TZP-III; (d) Ce-TZP-IV.

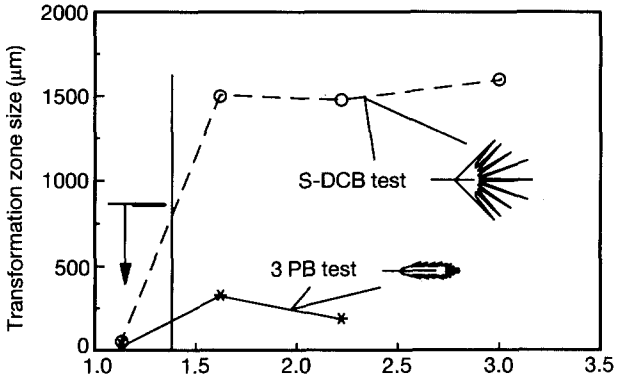

Figure 5 Grain-size and specimen-size dependence of the size and shape of the transformation zone.

Fig. 11 shows the crack-resistance, J_R, curves for the Ce-TZPs with larger grain sizes and hence transformation zones. Because the transformation zone size is large relative to the specimen dimensions, K-characterization of crack growth is inappropriate and the J-integral approach has been used instead to describe the crack-resistance behaviour. Three important characteristics can be summarized in these J_R–Δa curves.

1. In the SENB specimens the J-integral values are overall much higher than the J_{el} values derived from the K_I values.

2. In the s-DCB specimens the J-integral values agree well with the J_{el} values for crack extension less than 1.5 mm, where the transformation zone size is still small compared to the specimen size. With increasing crack extension and larger transformation zones, however, the J-integral values become much higher than the J_{el} values. Thus the K concept is only valid for the s-DCB specimens, if the crack extension as well as the transformation zone size are small.

3. The J_R–Δa curves obtained from the SENB geometries show very different trends. The J_R–Δa curves for the SENB geometry show relatively higher starting values than the s-DCB geometries and tend to a plateau after a crack growth of 1–2 mm. However, the J_R-curves for the s-DCB specimen rise rapidly with crack growth with no apparent plateau value.

Fig. 12 shows the increase of the transformation zone size in the lengthwise direction for both the SENB and s-DCB specimens as a function of crack extension. Quite clearly, for the same amount of crack extension, the transformation zone size is much larger and the zone size increases much faster for the s-DCB than the SENB specimens.

4. Discussion

4.1. Grain-size effect on the transformation behaviour

Basically, both nucleation [19, 20] and local stress/strain [21, 22] are factors which contribute to

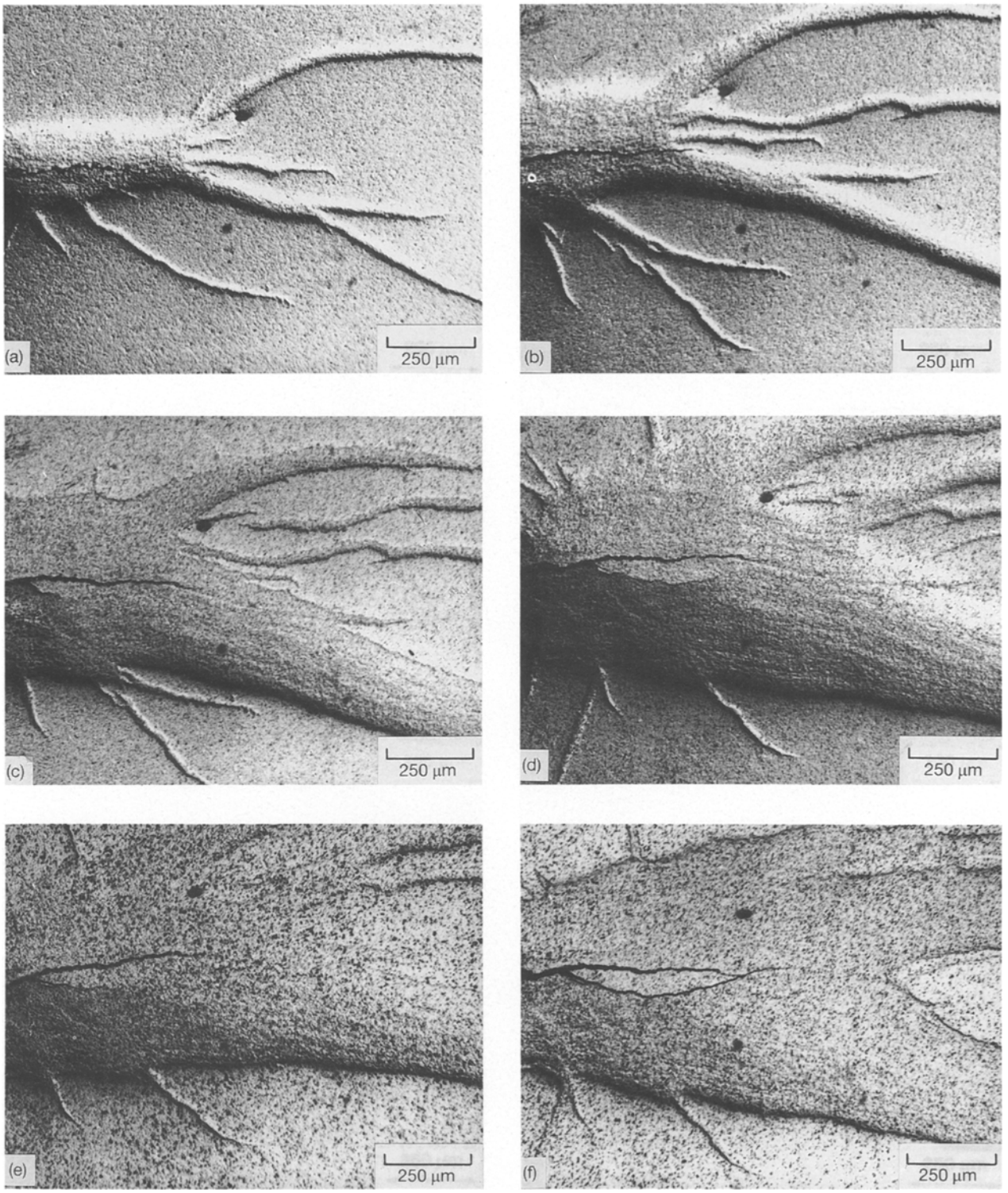

Figure 6 Development of the transformation zone during repeated loading/unloading of a Ce-TZP-II SENB specimen in three-point bending. n (number of cycles): (a) 1, (b) 2, (c) 3, (d) 4, (e) 5, (f) 6.

the observed precipitate/grain/particle-size dependence of the transformation of the tetragonal phase. The probability of a potential nucleus, one which will grow to critical size and allow the transformation to proceed, being present within a precipitate or grain increases with the volume of the tetragonal phase [19, 20]. It has also been observed that a grain-localized tensile stress can promote the t–m transformation [23, 24]. One important factor influencing this local stress condition is the local mismatch strains at grain boundaries due to the difference in the thermal expansion coefficients in the c- and a-axes of the tetragonal phase [21]. This anisotropy increases with increase in grain size [25, 26].

The grain-size effect on transformation and on transformation toughening has been investigated previously [9] on 12 mol % Ce-TZPs. It was found that the M_S temperature for the t–m transformation, the transformation zone size, h, and the transformation toughening, all increase continuously with grain size. These results are consistent with the theoretical analysis based on thermodynamics, especially the nuclea-

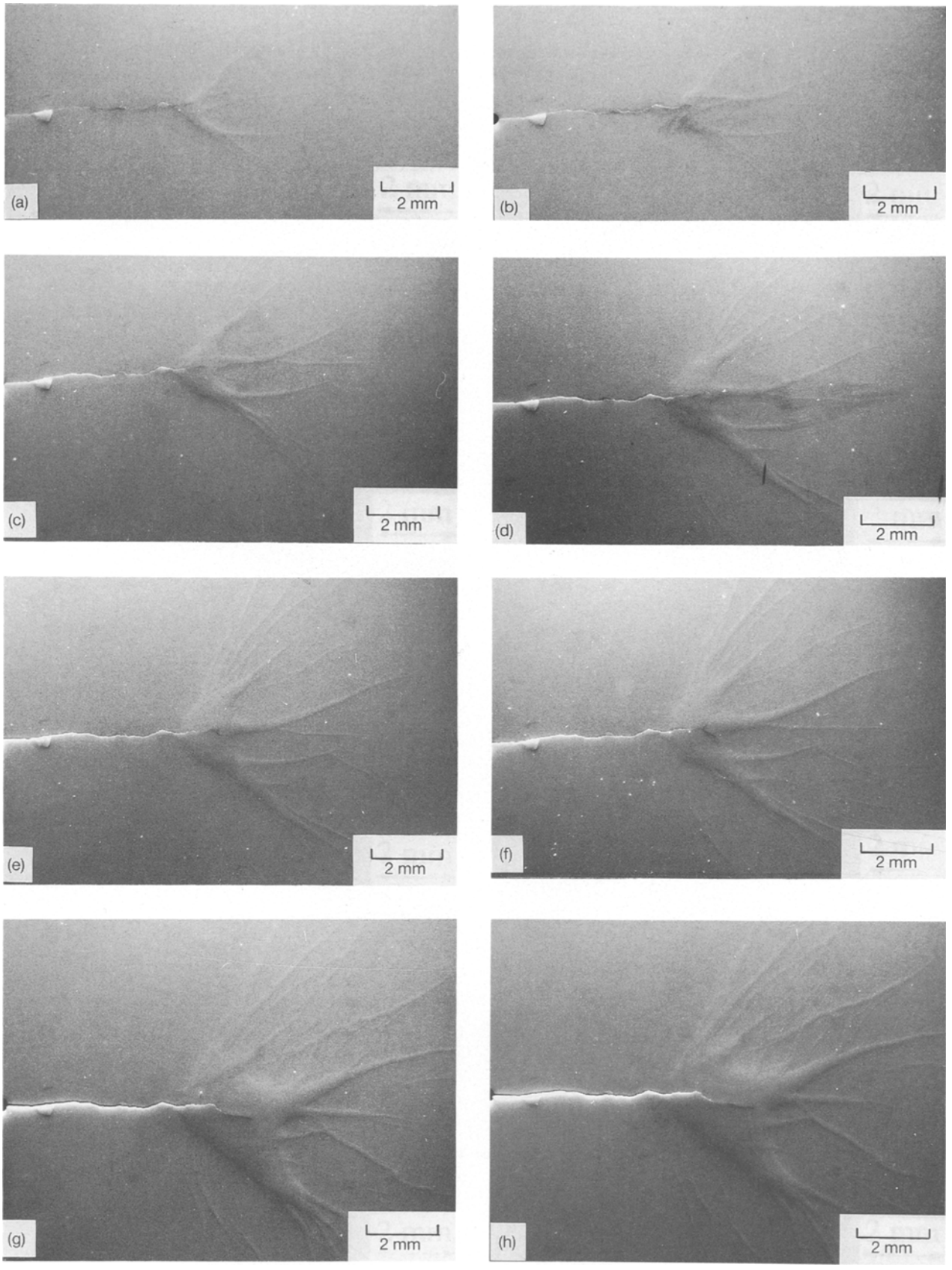

Figure 7 Development of the transformation zone during repeated loading/unloading of a Ce-TZP-III s-DCB specimen. *n* (number of cycles): (a) 6, (b) 9, (c) 13, (d) 17, (e) 19, (f) 22, (g) 26, (h) 30.

tion processes of the t–m transformation, as discussed above. The 9 mol% Ce-TZPs investigated here, however, show two different types of transformation behaviour: a very limited transformation zone with a grain size of 1.1 μm and a very large transformation zone for grain sizes of 1.6, 2.2 and 3 μm (see Figs 3–5). It is apparent that there is a critical grain size in the 9 mol% Ce-TZPs below which the "burst-like" (autocatalytic) t–m phase transformation cannot be initiated. Several factors should be considered to ex-

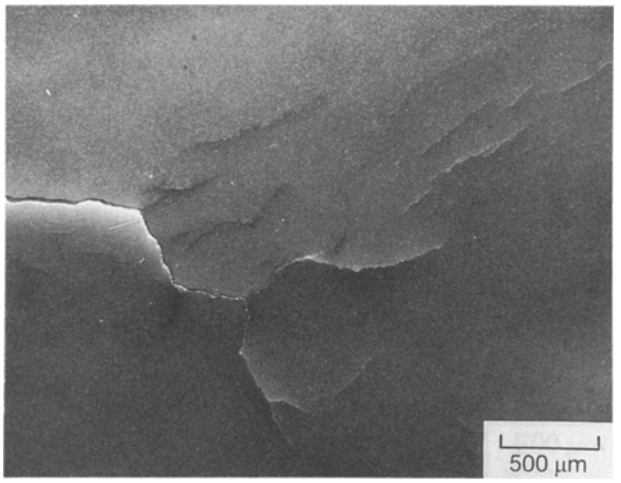

Figure 8 Microcracking in the t–m transformation zone of the Ce-TZP-IV material with a grain size of 3 μm.

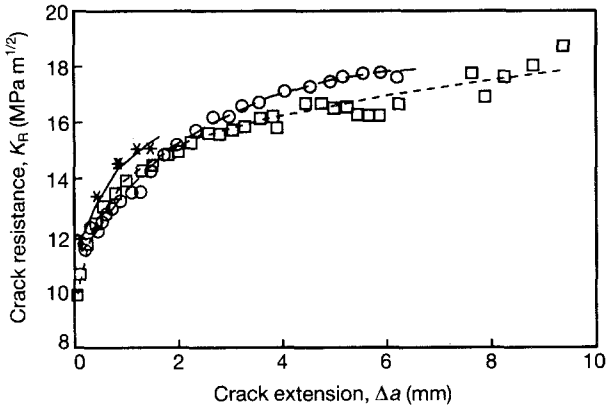

Figure 9 Crack-resistance curves. K_R, for Ce-TZP-I measured in (×) SENB and (○) s-DCB specimens. (□) CT specimen.

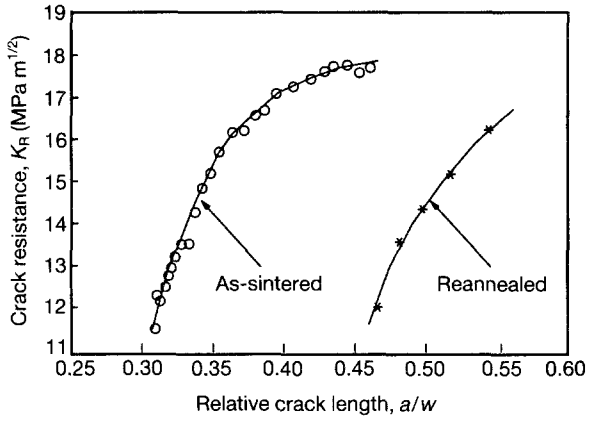

Figure 10 Crack-resistance curves, K_R, for Ce-TZP-I after reannealing in s-DCB specimens.

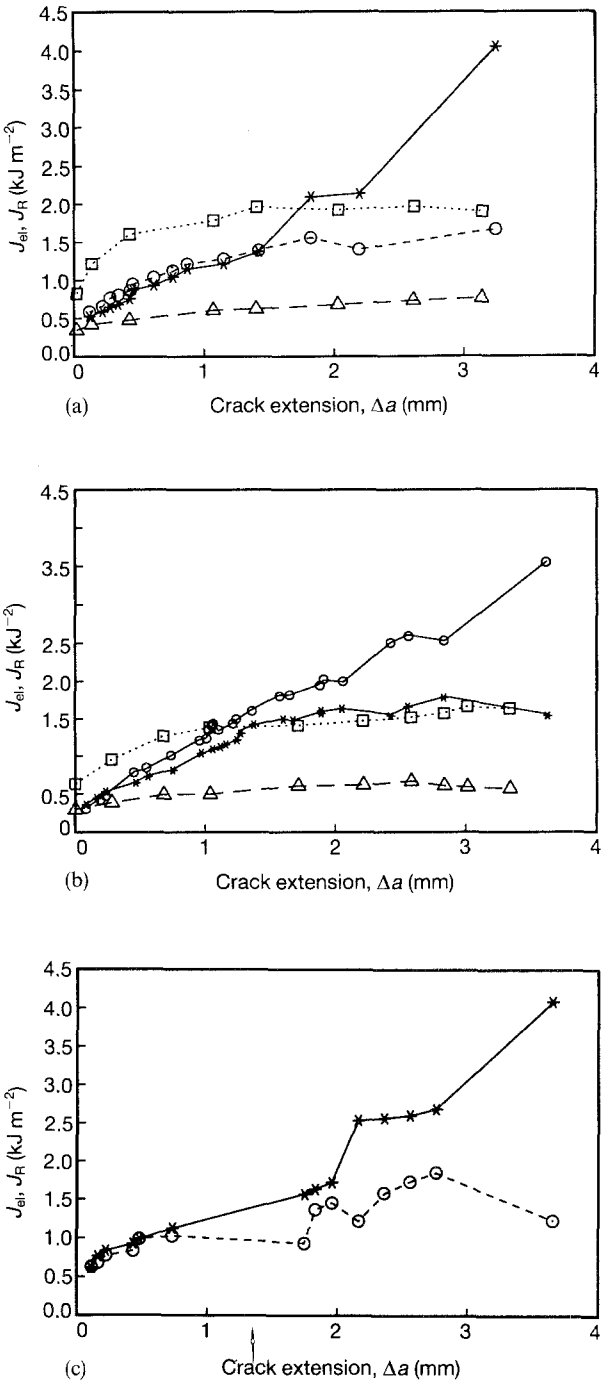

Figure 11 Crack-resistance curves, J_R, for (a) Ce-TZP-II, (b) Ce-TZP-III and (c) Ce-TZP-IV measured in (□, △) SENB and (×, ○) s-DCB specimens. Note that "autocatalytic transformation" and stepwise crack growth are demonstrated by the discontinuous segments of the J_R–Δa curves for the s-DCB specimens. (×, □) J_R, (○, △) J_{el}.

plain the different grain-size dependence of the t–m transformation behaviour in the 12 and 9 mol % Ce-TZPs. (1) The grain-localized tensile stress in the 9 mol % Ce-TZPs is higher than that in the 12 mol % Ce-TZPs because the thermal anisotropy increases with decreasing CeO_2 content in the ZrO_2. (2) The starting powder used in this work contains a minor amount of SiO_2 as a glassy phase. Its distribution within the grains and/or at the grain boundaries could vary with grain size when sintered at different temperatures. Consequently, this and other impurities may influence the transformation behaviour of the 9 mol % Ce-TZPs as the grain size is changed. It is noted that the 12 mol % Ce-TZPs investigated previously [9] is rather pure. (3) The distribution of cerium in ZrO_2 at different sintering temperatures has to be investigated as this may also influence the transformation behaviour. (4) In addition, the distribution of the amount of the t–m transformation within the transformation zone should be further investigated. It is also very

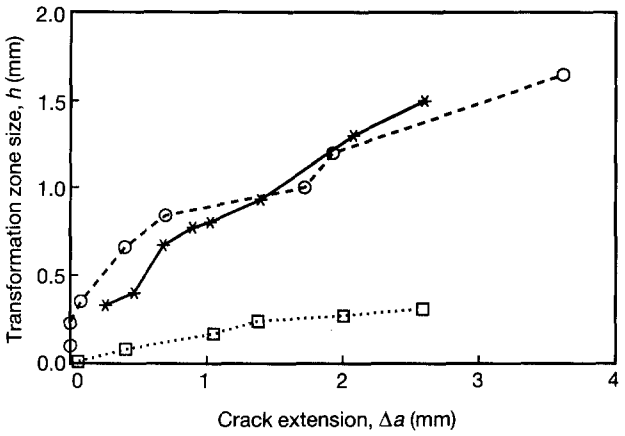

Figure 12 Lengthwise transformation zone size in (□) SENB and (x, ○) s-DCB geometries as a function of crack extension. (□) Ce-TZP-II, (○) Ce-TZP-IV, (×) Ce-TZP-III.

important to note that with increasing grain size "burst-like" t–m transformation behaviour has become more pronounced.

4.2. Specimen-geometry effect on transformation and *R*-curve behaviour

For the evaluation of valid plane strain K_I values, the crack length, a, thickness, t, and the ligament length, $w - a$, must satisfy the following requirements [27]

$$t, a, w - a > 50h \quad (8)$$

where h is the lengthwise transformation zone size. By comparison of Table II with Figs 5 and 12 it can be seen that for the Ce-TZP-I material plane strain and the small-scale yielding conditions are fully satisfied by both SENB and s-DCB specimens throughout the whole crack-growth process. However, for the larger grain-size materials, Ce-TZP-II, III and IV, except for the first couple of millimetres of crack extension, the specimen size and thickness are too small for valid K_I measurements in the s-DCB geometry. The SENB geometry is also not suitable to measure K_R–Δa curves in these three latter materials. It is hence necessary to determine the J_R–Δa curves for the Ce-TZP-II, III and IV ceramics using Equations 2 and 4 in accordance with the ASTM standard [13–16]. These J_R curves are already shown in Fig. 11 and only valid data points are given there. Difficulties in obtaining sufficiently large-size specimens have precluded the evaluation of K_R–Δa curves for these latter Ce-TZPs.

The J_R–Δa curves measured from the SENB and s-DCB specimens show that for identical materials the s-DCB geometry has a greater slope, dJ_R/da, than that for the SENB geometry caused by a much larger transformation zone size at a given crack growth (see also Fig. 12). Although the crack initiation J-values for the SENB geometry is larger than the s-DCB geometry we believe this may be associated with the accuracy in identifying the precise crack initiation points on the load versus load point displacement curves in the SENB test.

TABLE II Specimen thickness, t, crack length, a, and ligament length, $w - a$, of the SENB and s-DCB specimens

Specimen	t(mm)	a(mm)	$w - a$(mm)
SENB	5	3–7	7–3
s-DCB	6.5	15–20	25–20

To explain the differences in the transformation zone size (see Fig. 5) and crack-resistance curves (see Fig. 11) with different specimen geometry and size, we realize that the states of stress in these two specimen types are quite different. While the thickness of the SENB specimens does not satisfy the full plane strain condition according to Equation 8, they are not far from it. The s-DCB specimens, on the other hand, are hardly near plane strain and are closer to plane stress. These differences lead to different thickness constraint effects [28]. By analogy with crack-tip plastic deformation fields the relatively lower thickness constraint in the s-DCB geometry produces a larger transformation zone size. Also, although there are predominant bending stresses in the ligament of both specimen geometries there is an additional tensile stress acting perpendicular to the ligament of the s-DCB specimens. The transformation zone size and geometry are therefore expected to be larger in the s-DCB geometry and hence to give larger crack-resistance curves. However, further theoretical analysis is needed to understand the correlations between the transformation zone size, the stress state and the constraint effect. In particular the formation and size of the "tails" due to the "autocatalytic" effect in the SENB and s-DCB geometries have to be fully explained. The through-thickness transformation zones also have to be investigated further.

5. Conclusion

Two types of transformation behaviour are observed in the 9 mol % Ce-TZP ceramics: one is a small line shaped transformation zone with a continuous load–load point displacement curve for a grain size of 1.1 μm; the other is a very large transformation zone associated with a "burst-like" (autocatalytic) transformation behaviour and a discontinuous stepwise load–load point displacement curve for the other materials with grain sizes larger than 1.5 μm.

There is also a pronounced specimen geometry effect on the t–m transformation zone in these materials both in shape and in size. For example, the transformation zone size of the short-DCB geometry is about three to five times larger than that of the SENB geometry at identical crack extension. This is thought to be caused largely by the differences in the stress state and the thickness constraint between the two specimen types.

For the Ce-TZP-I with a grain size of 1.1 μm and a very small t–m transformation zone, the crack-resistance can be characterized successfully using the K concept. The K_R curves measured in SENB, s-DCB and CT specimens show very good agreement. How-

ever, for the other three materials with grain sizes in the range of 1.6–3.0 μm and very large transformation zones, the J_R-curve approach has to be used to characterize their crack-resistance behaviour. The J_R–Δa curves measured experimentally are dependent on specimen geometry because the transformation zones in the SENB and s-DCB specimens are dissimilar.

Acknowledgement

The authors thank the Australian DITAC Industry Research Development Board, Manufacturing and Materials Technology Grant 15042, and the MWK Baden-Wuerttemberg under the KKS-funding, Keramikverbund Karlsruhe-Stuttgart, Germany, for the financial support of this work.

References

1. R. M. McMEEKING and A. G. EVANS, *J. Am. Ceram. Soc.* **65** (1982) 242.
2. B. BUDIANSKY, J. W. HUTCHINSON and J. C. LAMBROPOULOS, *Int. J. Solid. Struct.* **19** (1983) 337.
3. D. B. MARSHALL and M. V. SWAIM, *J. Am. Ceram. Soc.* **71** (1988) 399.
4. R. W. STEINBRECH and A. H. HEUER, *Mater. Res. Soc. Symp. Proc.* **60** (1986) 469.
5. N. CLAUSSEN, *J. Am. Ceram. Soc.* **59** (1976) 49.
6. G. GRATHWOHL and T. LIU, *ibid.* **74** (1991) 318.
7. L. R. F. ROSE and M. V. SWAIN, *Acta Metall.* **36** (1988) 955.
8. C.-S. YU and D.-K. SHETTY, *J. Am. Ceram. Soc.* **72** (1989) 921.
9. G. GRATHWOHL and T. LIU, *ibid.* **74** (1991) 3028.
10. R. WARREN and B. JOHANNESSON, *Powder Metall.* **27** (1984) 25.
11. W. F. BROWN and J. E. SRAWLEY, in "Plane-Strain Crack Toughness Testing of High Strength Metallic Materials", ASTM Special Technical Publication, 410 (American Society for Testing and Materials, Philadelphia, PA, 1966) p. 13.
12. W. K. WILSON, *Eng. Fract. Mech.* **2** (1970) 169.
13. S. J. GARWOOD, J. N. ROBINSON and C. E. TURNER, *Int. J. Fract.* **11** (1975) 528.
14. J. E. SRAWLEY and GROSS, *Eng. Fract. Mech.* **4** (1972) 587.
15. "Standard Test Methods for J_{Ic}, A Measure of Fracture Toughness", Designate, E813 817 (Associated Board of ASTM Standards, Philadelphia, PA, 1988) pp. 686–700.
16. H. A. ERNST, P. C. PARIS and J. D. LANDES, in "Fracture Mechanics", ASTM STP 743, edited by R. Roberts (American Society for Testing and Materials, Philadelphia, PA, 1981) pp. 476–507.
17. E. INGHELS, A. H. HEUER and R. STEINBRECH, *J. Am. Ceram. Soc.* **73** (1990) 2023.
18. A. H. HEUER, N. CLAUSSEN, W. M. KRIVEN and M. RUEHLE, *ibid.* **65** (1982) 642.
19. I.-W. CHEN and Y. H. CHIAO, *Acta Metall.* **29** (1981) 447.
20. S. SCHMAUDER and H. SCHUBERT, *J. Am. Ceram. Soc.* **69** (1986) 534.
21. M. RUEHLE and W. M. KRIVEN, *Ber. Bunse. Phys. Chem.* **87** (1983) 222.
22. R. H. J. HANNINK, *J. Mater. Sci.* **18** (1983) 457.
23. A. H. HEUER and R.-R. LEE, *Rev. Phys. Appl.* **23** (1988) 565.
24. M. K. FERBER, P. F. BECHER and C. B. FINCH, *J. Am. Ceram. Soc.* **66** (1983) C2.
25. R. W. RICE and R. C. POHANKA, *ibid.* **62** (1979) 559.
26. A. G. ATKINS and Y.-W. MAI, "Elastic and Plastic Fracture: Metals, Polymers, Ceramics, Composites" (Ellis Harwood, Chichester, UK, Halstend Press, NY, 1985).
27. "Standard Test Method for Plane-Strain Fracture Toughness of Metallic Materials" ASTM Designation: E 399-90^{E1} (American Socity for Testing and Materials, Philadelphia, PA) Annual Book of ASTM Standards, edited by P. C. Fazio *et al.* **3.01** (1992) pp. 518–54.
28. Y. W. MAI and B. LAWN, *Ann. Rev. Master. Sci.* **16** (1986) 415.

Received 6 April 1993
and accepted 3 June 1993